

Full scale testing of unreinforced masonry walls with openings



F. Parisi, N. Augenti, A. Prota & G. Manfredi

Department of Structural Engineering, University of Naples Federico II, Naples, Italy

SUMMARY:

Full scale lateral loading tests on unreinforced masonry walls with an opening are presented. The main scope of the experimental program was to investigate the role of spandrels and their interaction with piers. The specimens were subjected to displacement-controlled quasi-static lateral force under constant vertical forces on piers and were composed by two piers connected by a spandrel panel. The contribution of the following spandrel configurations was investigated: (1) spandrel with wooden lintel above the opening; (2) spandrel with masonry arch above the opening and reinforced concrete bond beam at the top. A composite strengthening system was also applied on both sides of the first spandrel type to assess its effectiveness in seismic upgrading and quick repair/remedial measures during earthquake sequences. In all cases nonlinear behaviour of specimens was significantly affected by rocking of piers and heavy damage to spandrels, which allowed satisfactory specimen re-centring and large displacement capacity.

Keywords: composites, full scale testing, spandrels, unreinforced masonry walls with openings

1. INTRODUCTION

In the last decade full scale testing programs have become an important reality in earthquake engineering research, leading to a number of laboratory networks at both national and international levels. In the case of masonry constructions full scale testing is the unique solution to validate/calibrate analysis procedures and to assess new strengthening techniques, because their structural behaviour is nonlinear even at small deformation levels and hence similitude theory does not apply. Past shaking table tests have shown that nonlinear behaviour of masonry buildings is significantly affected by the amount of damage to spandrels, which are the horizontal masonry strips between openings of consecutive storeys (Augenti 2000). If such a damage is heavier than that to piers (i.e., vertical masonry components), energy dissipation capacity provides satisfactory earthquake resistance to the unreinforced masonry (URM) building (Benedetti et al. 2001). Although spandrels play a key role in seismic behaviour of masonry buildings, until now research has been mainly focused on the in-plane behaviour of piers (Magenes and Calvi 1997) whose failure prior to that of spandrel induces a premature building collapse. This lack of knowledge is reflected by current seismic codes, such as Eurocode 8 (CEN 2005), FEMA 356 (ASCE 2000) and Italian building code (IBC) (IMIT 2008), which do not provide specific criteria for modelling and safety verification of spandrels.

A remarkable knowledge advance on spandrels has been reached in the frame of ReLUIS-DPC 2005–2008 project by means of analytical, numerical and experimental studies (Augenti et al. 2011, Gattesco et al. 2010, Magenes et al. (in print)). The authors carried out a first series of in-plane lateral loading tests on a masonry wall with an opening, which were performed in a quasi-static fashion and displacement control. The experimental program continued with an additional full scale lateral loading test on a masonry wall with the same geometry, simulated gravity loads and material properties of that previously tested, but with a different spandrel type. The main scope of this experimental program was to assess the contribution of spandrels to nonlinear behaviour of masonry buildings for different

spandrel configurations. This paper is aimed at presenting experimental results provided by the last test, which are compared to those discussed by the authors in previous works in order to identify similarities and differences in terms of observed crack patterns and force–displacement diagrams. It is underlined that this experimental program deals with tuff masonry constructions which are mainly located in Mediterranean countries and often belong to cultural heritage. Tuff masonry is composed by tuff stones and mortar joints, and is affected by high porosity. Given that such constructions often lie in earthquake-prone regions, they are to be preserved according to worldwide guidelines and principles for cultural heritage preservation.

2. EXPERIMENTAL PROGRAM

In-plane lateral loading tests were performed on two tuff masonry walls with an opening. Such specimens were supposed to be taken out from typical multi-storey walls with a series of vertically-aligned openings. Specimen #1 had a wooden lintel above the opening whereas specimen #2 had a masonry arch above the opening and a reinforced concrete (RC) bond beam at the top of the spandrel.

Lateral loading tests of specimen #1 were performed in as-built, pre-damaged and repaired-upgraded conditions. The first lateral loading test was conducted on the as-built specimen #1 in order to investigate nonlinear response up to the first significant cracking (i.e., permanent damage) in the spandrel. A second test was carried out on the pre-damaged specimen #1 attempting to assess residual response properties of pre-damaged URM buildings located in earthquake-prone regions. This is a very important task because: (1) many buildings damaged by past earthquakes have not yet been repaired until now, so their seismic capacity should be estimated by considering potential effects of previous damage; (2) cumulative damage should also be considered in seismic capacity models of URM buildings subjected to earthquake sequences. Finally, specimen #1 was first repaired by filling cracks with mortar and replacing some stones of piers, and then it was upgraded by applying an inorganic matrix-grid (IMG) composite strengthening system on both sides of the spandrel. The use of a mortar-based matrix was preferred over resin-based matrices because it has higher compatibility with the tuff masonry substrate, lower sensitivity to high temperatures and lower flammability (Prota et al. 2006). Therefore, the last test was performed on the IMG-repaired specimen #1 up to a near-collapse state in order to assess the effectiveness of the proposed strengthening technique for retrofit/upgrading of URM structures and fast remedial works during seismic emergency scenarios. That test was also aimed at confirming that the IMG strengthening system installed on masonry spandrels could allow improving their energy dissipation capacity, according to suggestions by Benedetti et al. (2001). At the same time, the IMG strengthening system was also chosen to ensure structural upgrading in compliance to principles of minimum intervention and reversibility, that are mandatory for historical buildings.

Specimen #2 was subjected to in-plane lateral loading until a near-collapse state was reached, namely, a heavy damage to both piers and spandrel was observed. All tests on both specimens were carried out in quasi-static fashion and displacement control to investigate nonlinear behaviour at increasing deformation demands, including post-peak softening branch of force–displacement diagrams.

2.1. Material properties

Mechanical properties of the constituent materials of both tuff masonry and the IMG strengthening system were firstly determined through several laboratory tests (Augenti and Parisi 2010). Unit weight of tuff masonry was 16 kN/m^3 while two limit mean values of shear strength at zero confining stress were assumed because such a strength was not experimentally characterized: $\tau_{0,min} = 0.05 \text{ MPa}$ and $\tau_{0,max} = 0.10 \text{ MPa}$. Minimum shear strength was derived from statistical analysis of experimental data on single-leaf tuff masonry assemblages (Augenti and Parisi 2009) provided by MADA (Masonry Database), an online database for mechanical modelling of masonry (Augenti et al. 2012) [URL: http://www.reluis.it/index.php?option=com_mada&Itemid=156]. Tuff masonry was realized with

yellow tuff stones (150×300×100 mm in size) and a hydraulic mortar composed by natural sand and pozzolana-like reactive aggregates with 1:6.25 water/sand ratio by weight. Tuff stones were characterized through uniaxial compression tests on cubic specimens of edge length 70 mm, while mortar was characterized through similar tests on specimens 40×40×160 mm in size. Augenti and Parisi (2010) also estimated mechanical properties of the entire tuff masonry through two series of uniaxial compression tests along the directions parallel and orthogonal to the mortar bed joints of prisms (610×650×150 mm in size). The tuff units used for masonry prisms had the same size of those employed for wall specimens and were bonded each other through pozzolana-like mortar joints of thickness 10 mm. The used mortar is classified as M2.5 by IBC (IMIT 2008), while the whole tuff masonry exceeded the reference interval of [1.4 MPa, 2.4 MPa] suggested by IBC for existing masonry buildings in the absence of specific mechanical characterization tests.

The fibre-reinforced composite material employed for external strengthening of specimen #1 consisted of a special two-component inorganic matrix and a glass fibre net. The former was made of hydraulic lime and sand (ratio by weight 1:3) added with glass fibres (ratio by total weight 1:10) and mixed with latex and water (ratio by weight 2:1). The glass fibre-reinforced matrix ensured higher ductility and tensile strength, resulting in a high-performance composite. The grid was a bidirectional alkali-resistant glass coated net with 25×25 mm texture, 225 g/m² unit weight, and 1.77% ultimate strain. Material properties of both masonry and IMG strengthening system are outlined in Table 2.1.

Table 2.1. Material properties

Material	f_i [MPa]	f_c [MPa]	E [GPa]	G [GPa]
Tuff stones	0.23	4.13	1.54	0.44
Pozzolana-like mortar	1.43	2.50	1.52	0.66
Tuff masonry (compression to bed joints)	–	3.85	2.07	0.86
Tuff masonry (compression ⊥ to bed joints)	–	3.96	2.22	0.92
IMG system matrix	6.00	16.0	8.00	–
IMG system grid	1276	–	72.0	–

2.2. Geometry of specimens

Both specimens' geometry and test setup were designed in a way to avoid any predefined boundary condition for the spandrel and to develop most part of damage within the spandrel panel above the opening. Static pushover analysis based on macro-element modelling of specimens was carried out to predict lateral load-bearing capacity considering monotonic behaviour of URM walls with openings (Parisi 2010). Namely, three types of macro-element were identified: two pier panels; a spandrel panel; and two joint panels. In the case of regular walls with openings, pier panels are vertical macro-elements with height equal to or greater than that of adjacent openings, spandrel panels are horizontal macro-elements with the same length of openings, and joint panels are identified by the intersection of piers and spandrels. Pier and spandrel panels are assumed to be flexible macro-elements whose capacity modelling is based on limit strength domains and mechanics-based force–displacement diagrams derived from direct integration of both bending and shear curvatures (Parisi and Augenti 2012). Joint panels are assumed to be rigid macro-elements with infinite resistance.

Figure 1 shows specimen #1 in both as-built and IMG-repaired conditions. Specimen #1 was a single-leaf, running bond, tuff masonry wall with a spandrel panel resting on a wooden lintel. The lintel had an anchorage length of 150 mm in both piers (Fig. 1a). The specimen was globally 5.10 m long, 3.62 m high and 0.31 m thick. To apply axial forces to the piers ensuring structural continuity with an ideal overlying storey, three masonry layers were constructed over the piers. Both piers and the spandrel panel had a length of 1.70 m, while the height of the spandrel panel was equal to 1.00 m. Masonry layers were alternated each other to get discontinuous vertical mortar joints of thickness

10 mm. The IMG strengthening system on specimen #2 was applied on both sides of the spandrel in order to ensure good anchorage to both piers (Fig. 1b). The IMG composite was selected because it does not increase inertia masses, allowing negligible changes in the stiffness distribution of URM buildings. The realization of the IMG strengthening system on each spandrel face consisted of three stages: masonry pre-wetting and first coating with 5 mm thick mortar layer; hand-pressing of IMG system grid into the wet binder with fibres aligned to mortar bed joints of the spandrel (overlapping length of grids set to 100 mm); and second coating with 5 mm thick mortar layer. The nominal thickness of the IMG strengthening system was then 10 mm on each spandrel face.

Figure 2 shows specimen #2 where a masonry arch, instead of a wooden lintel, was realized over the opening and a RC bond beam was cast in place at the top of the spandrel. Global dimensions of specimen #2 were equal to those of specimen #1. The RC bond beam cross section was 310×230 mm; type C20/25 concrete and type B450C reinforcing steel bars were used (CEN 1993). The beam was reinforced with four 14 mm diameter longitudinal steel bars and 8 mm diameter stirrups with 2 legs and 200 mm spacing.

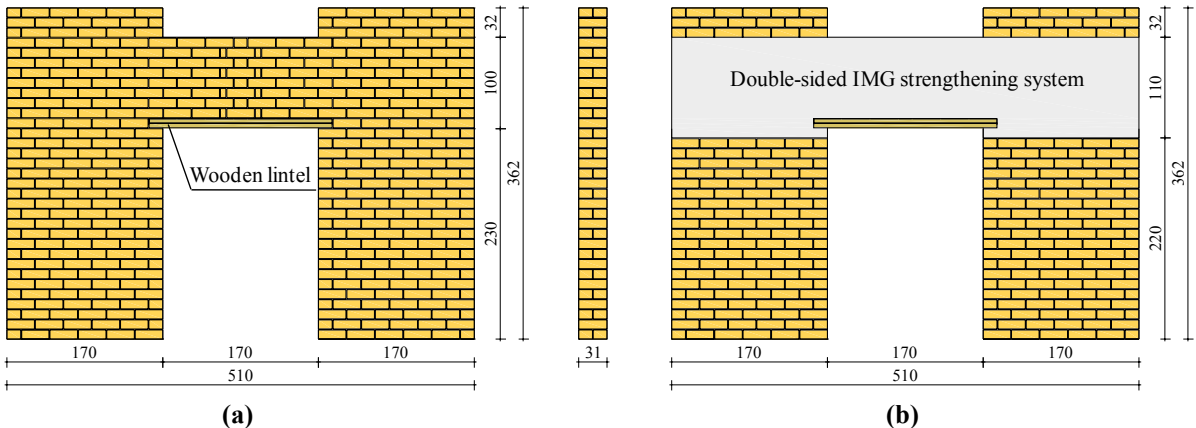


Figure 1. Specimen #1: (a) as-built; (b) IMG-repaired (dimensions in cm)

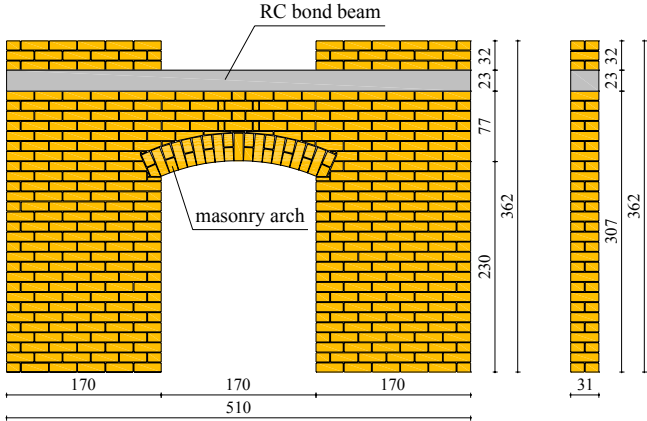


Figure 2. Specimen #2 (dimensions in cm)

2.3. Test setup and instrumentation

Figure 3 shows the experimental setup employed for lateral loading tests. Both specimens were rigidly connected to the laboratory strong floor by means of RC beams with dimensions 1700×310×200 mm, which were cast to Ω-shaped steel plates. The latter were bolted in turn to squared holes of the laboratory strong floor. Transverse frames were installed over the piers to provide reaction against vertical loading applied at the piers' centrelines by hydraulic jacks with 500 kN nominal capacity.

Rigid steel beams were placed above the piers to ensure their uniform loading and then two Teflon, that is, polytetrafluoroethylene (PTFE), layers were installed between hydraulic jacks and rigid beams to minimise friction at their interface. A non-prismatic reaction wall was anchored to the laboratory strong floor to provide reaction against lateral loading. The latter was applied through a servo-controlled hydraulic actuator with 500 kN nominal capacity and ± 250 mm stroke. A suspension system was installed to provide further support to the actuator. Six steel bars (18 mm in diameter) were employed to allow lateral force reversals for cyclic tests only. Finally, steel beams were bolted to transverse reaction frames at both specimen sides to prevent potential out-of-plane failure modes. A load cell with 200 kN nominal capacity and approximately 250 kN maximum capacity was positioned at the actuator end in order to measure lateral force.

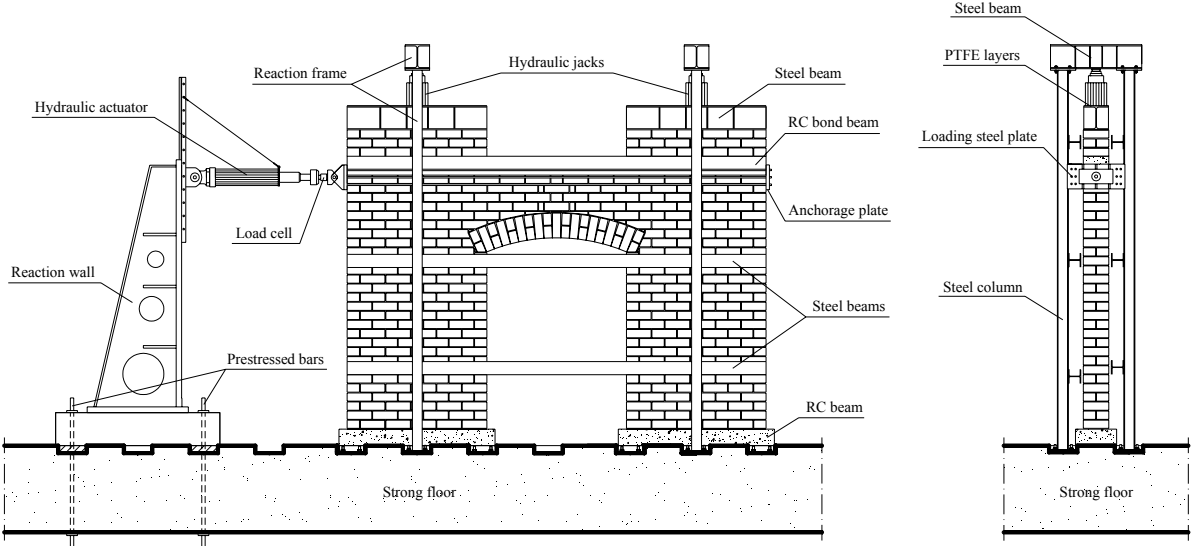


Figure 3. Test setup

Linear variable differential transformers (LVDTs) and potentiometer transducers (PTs) were installed. In the case of specimen #1 (Figs. 4a–b), LVDTs were placed at the end cross-sections of the spandrel and pier panels to obtain information about flexural deformations. PTs were mounted along both pier and spandrel diagonals to capture shear deformations. Joint panels were not instrumented as their behaviour was expected to be rigid owing to the specimen geometry (assumption confirmed by tests). Lateral displacements were measured at the opposite side with respect to the actuator through a potentiometer tagged as PT #1. Displacement readings at PT #1 were associated with lateral force readings at the load cell to plot force–displacement diagrams. The aforementioned readings were considered to be more accurate than load and stroke readings at the horizontal actuator.

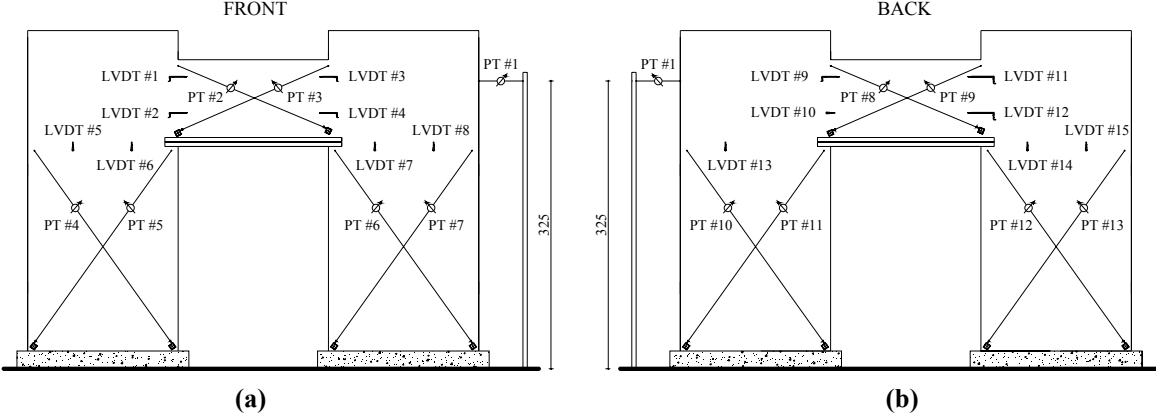


Figure 4. Instrumentation of specimen #1: (a) front side; (b) back side

Figure 5 shows the instrumentation of specimen #2, which was rather different from that of specimen #1 because the authors decided to perform a deeper investigation on rocking-induced displacements of piers and deformations of the RC bond beam. Rocking deformations of specimen #2 were measured through four vertical LVDTs at pier bases on the front side and four vertical PTs on the back side, which were fixed to RC beams to include the width of rocking-induced cracks at the pier bases.

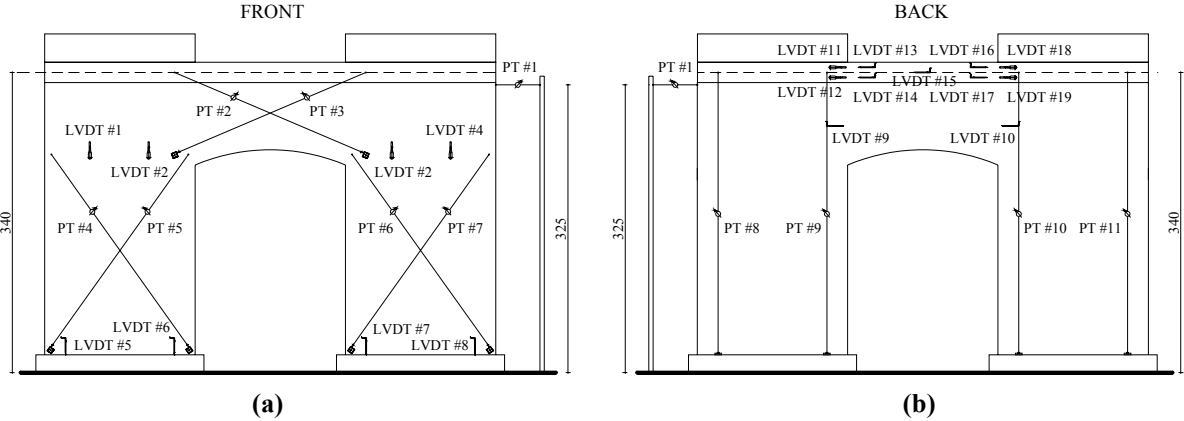


Figure 5. Instrumentation of specimen #2: (a) front side; (b) back side

2.4. Test procedures

Lateral loading tests consisted of two stages: application of 200 kN vertical forces over piers; and application of displacement-controlled horizontal force under constant vertical forces. Lateral force was modulated by the computer program of the data acquisition system in a way to obtain the target displacement time-history. All measurements were recorded at a sampling rate of 5 Hz. The as-built specimen #1 was tested under monotonically-increasing displacements, after two initial displacement cycles were applied to get a satisfactory contrast between specimen and actuator. Lateral loading was applied in a way to increase displacements at a constant rate $v = 0.01$ mm/s up to a displacement reading at the actuator of 28 mm (corresponding to an interstorey drift ratio, θ , of about 1% and a first significant damage to the spandrel). The pre-damaged specimen #1 was then tested under cyclic displacements at $v = 0.35$ mm/s in a way to attain increasing amplitudes in seven different blocks and repeated three times at each amplitude peak, up to almost the same target displacement ($d = 39.2$ mm) and drift ($\theta = 1.2\%$) reached in the monotonic test. The displacement increment between consecutive displacement terns was set to 5.6 mm. The IMG-repaired specimen #1 was tested under fifteen cyclic displacement blocks up to $d = 84$ mm ($\theta = 2.8\%$). In that case the displacement rate was set to 0.35 mm/s in the first seven blocks and 0.70 mm/s in the last eight blocks. Figure 6a shows displacement time-histories employed for cyclic tests on specimen #1.

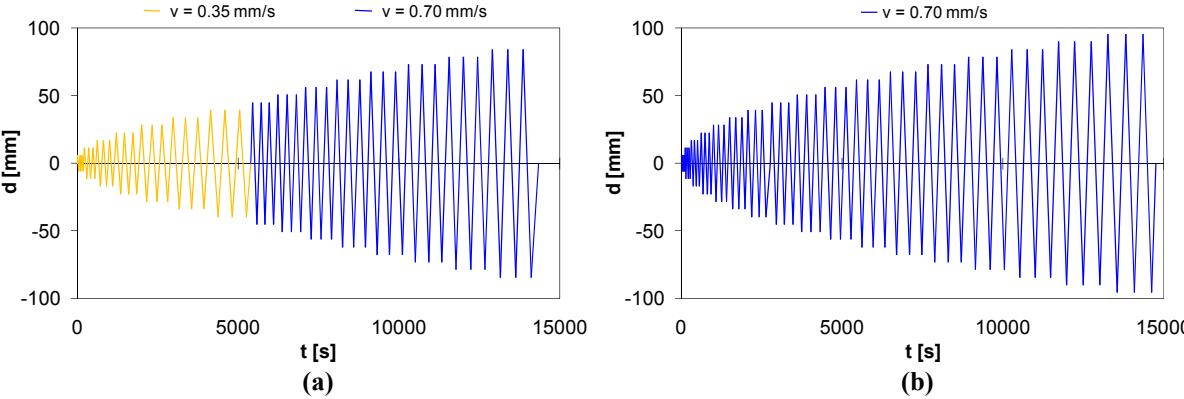


Figure 6. Displacement time-histories of cyclic tests: (a) specimen #1; (b) specimen #2

Specimen #2 was cyclically tested under seventeen cyclic displacement blocks (i.e., 51 cycles) up to $d = 95.2$ mm (namely, $\theta = 2.9\%$). The displacement rate and increment were set to 0.70 mm/s and 5.6 mm, respectively, as shown in Figure 6b.

3. DAMAGE PATTERNS

Detailed information on damage patterns related to specimen #1 was provided by Augenti et al. (2011). Here the authors recall observed damage to the spandrel panel of specimen #1 to compare it with that observed on specimen #2. The spandrel panel suffered diagonal shear cracking and slight flexural cracks at end sections in both as-built and pre-damaged conditions of specimen #1 (Figs. 7a–b) at θ_{max} equal to 0.9 and 1.1%, respectively. Conversely, extensive horizontal cracking associated with bending and masonry splitting was detected on the IMG-repaired spandrel panel at an actual drift $\theta_{max} = 2.5\%$ (Fig. 7c). Based on experimental-analytical comparisons, Parisi et al. (2011) showed that such a transition from shear to flexural failure occurred because the IMG strengthening system caused a shear strength increase significantly greater than flexural strength increase. Transverse connection between IMG system layers throughout the spandrel panel would have probably increased flexural strength of the spandrel panel, avoiding masonry splitting and resulting in greater load-bearing capacity of URM walls with openings. The masonry arch and RC bond beam in the spandrel panel of specimen #2 induced a considerably different damage at $\theta_{max} = 2.9\%$, which was the result of the following progressive damage: formation of axial cracks in the arch at $\theta = 0.69\%$; collapse of a little arch portion in the middle at $\theta = 0.86\%$; collapse of an arch wedge at $\theta = 1.03\%$ after piers begun to experience rocking rotations; collapse of second arch portion at $\theta = 1.21\%$ along with early crushing and splitting of piers at their base; collapse of fourth arch portion at $\theta = 1.72\%$ along with early cover ejection from the RC bond beam at the upper edge of end section; complete concrete cover ejection at $\theta = 2.58\%$; collapse of first and second masonry layers above the arch at the first and second displacement cycles, respectively, at $\theta = 2.76\%$ together with plastic hinging in the RC beam.

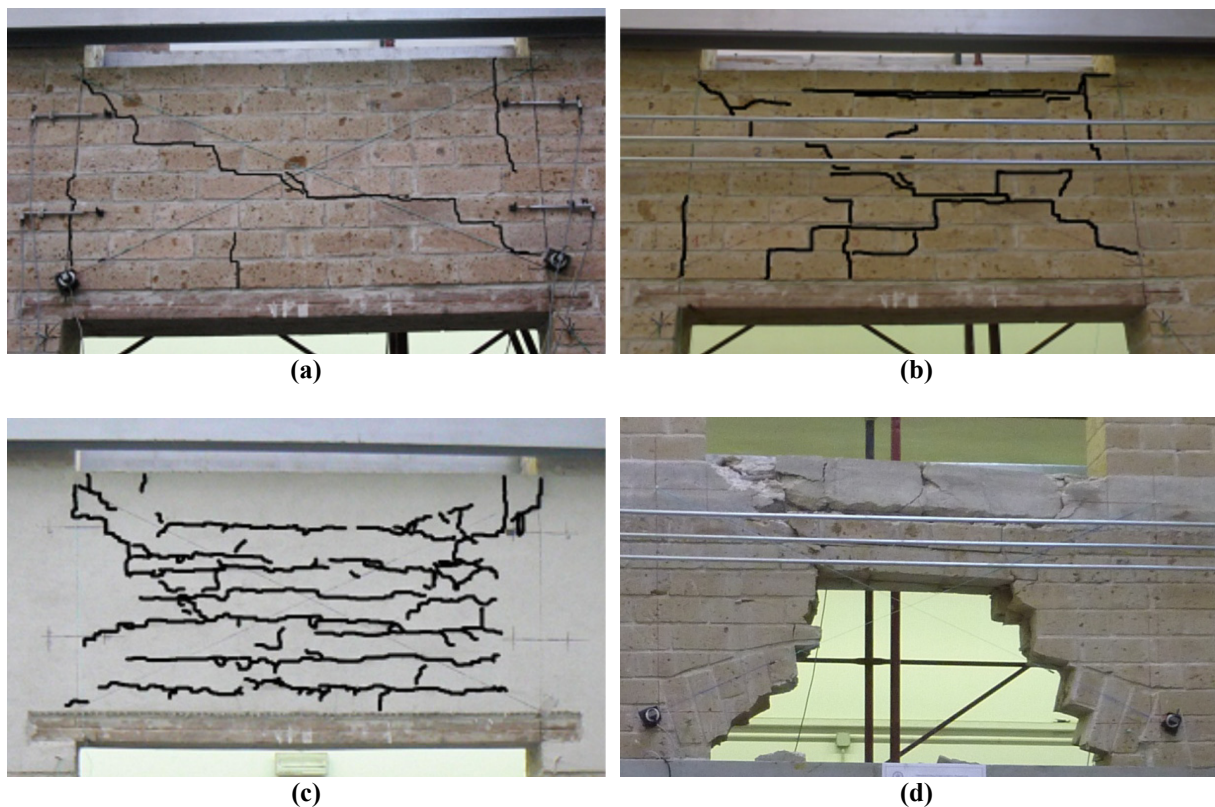


Figure 7. Damage to spandrel panel at maximum drifts: (a) as-built specimen #1 ($\theta_{max} = 0.9\%$); (b) pre-damaged specimen #1 ($\theta_{max} = 1.1\%$); (c) IMG-repaired specimen #1 ($\theta_{max} = 2.5\%$); (d) specimen #2 ($\theta_{max} = 2.9\%$)

In all cases rocking rotations of piers increased with the global drift demand on specimens. Rocking-induced horizontal cracks at the pier bases which exceeded 25 mm in the case of IMG-repaired specimen #1 and 30 mm in the case of specimen #2 (Figs. 8a–b). Rocking of piers induced large drift demands on spandrel panels and hence heavy damage to them. Collapse of specimens was thus observed after masonry crushing at the pier bases. Figures 9a and 9b show global damage to the IMG-repaired specimen #1 and specimen #2, where crushing of piers was significant. In the case of specimen #2, progressive damage to the spandrel induced gradual reduction in both height and effective length of the spandrel panel.



Figure 8. Rocking induced crack at pier base of specimen #2 ($\theta = 2.24\%$): (a) front view; (b) crack width



Figure 9. Overall damage at maximum lateral drift: (a) IMG-repaired specimen #1; (b) specimen #2

4. FORCE-DISPLACEMENT DIAGRAMS

Post-processing of experimental data allowed to obtain force (H) versus displacement (d) diagrams of specimens. A comparative analysis of such diagrams is here performed, whereas additional information on their bilinear idealisation for the computation of overstrength ratio, ductility and force-reduction factor, can be found in the work by Augenti et al. (2011). Fig. 10a shows a bilinear force–displacement behaviour up to a displacement $d = 19.74$ mm corresponding to $H_{max} = 184$ kN and $\theta = 0.65\%$, which caused shear cracking in the spandrel panel and the associated 15% lateral resistance drop. Another strength increase was measured up to $\theta_{max} = 0.9\%$. The experimental lateral resistance H_{max} confirmed the value provided by macro-element analysis of the as-built specimen ($H_{max} = 185$ kN) for the minimum shear strength of masonry ($\tau_{0,min} = 0.05$ MPa). The pre-damaged

specimen #1 had a maximum lateral resisting force approximately equal to that of the as-built specimen #1 at the occurrence of diagonal cracking in the spandrel panel, that is, 157 kN (Fig. 10b). This indicates that previous shear cracks in existing URM walls with openings could considerably affect the residual load-bearing capacity.

All lateral loading tests evidenced that the force–displacement behaviour (be it monotonic or cyclic) was clearly affected by rocking of piers, which allowed both re-centring (i.e., low residual displacements) and large displacement capacities of specimens. The IMG strengthening system let to restore the load-bearing capacity of the as-built specimen #1, shifting strength degradation at larger displacement levels (Fig. 10c). Load-bearing capacity of specimen #2 was $H_{max} = 224$ kN, that is, approximately 22% greater than that of as-built specimen #1 (Fig. 10d).

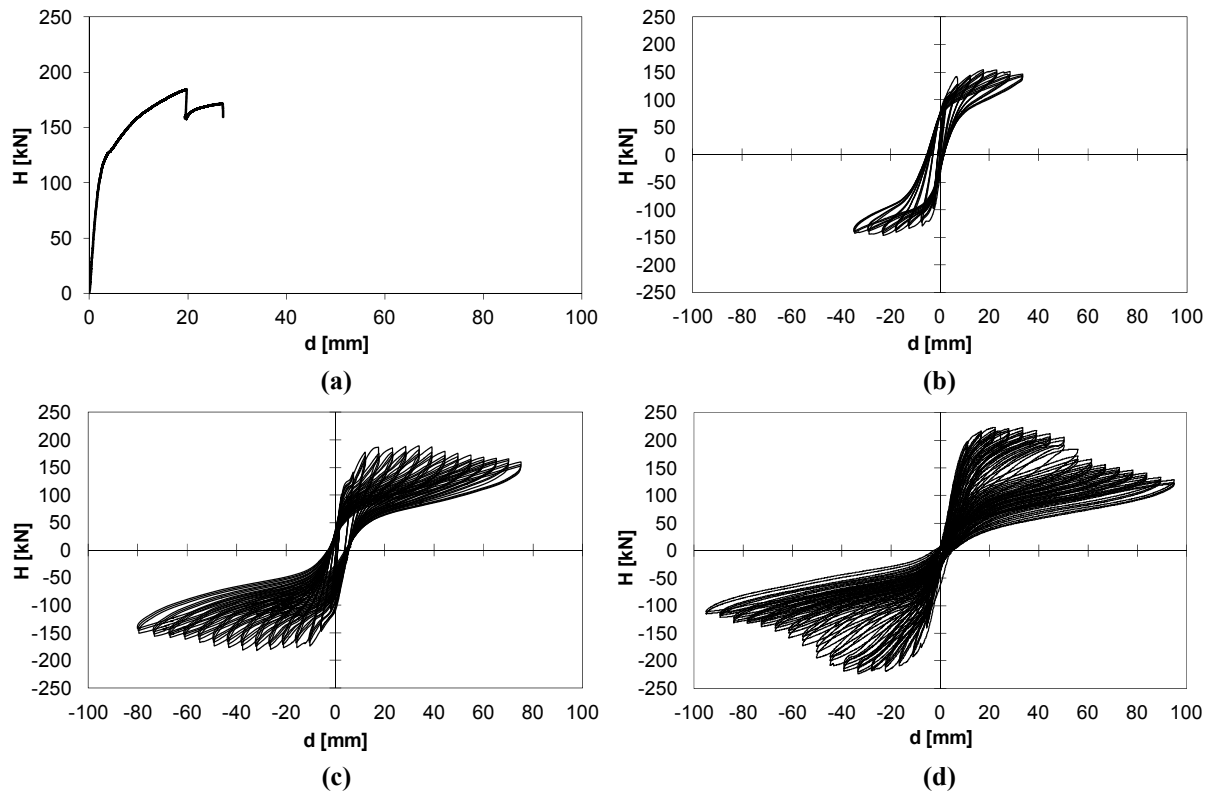


Figure 10. Force–displacement diagrams: (a) as-built specimen #1; (b) pre-damaged specimen #1; (c) IMG-repaired specimen #1; (d) specimen #2

5. CONCLUSIONS

Quasi-static lateral loading tests aimed at assessing the in-plane nonlinear behaviour of URM walls with openings have been presented. All tests showed that rocking behaviour of piers governed lateral stiffness of specimens, provided a stable hysteretic force–displacement behaviour, ensured both re-centring and displacement capacities, and induced larger drift demands on spandrel panels. No damage was detected in spandrel-pier nodal zones. Spandrel panels affected both lateral resistance and strength degradation of specimens and suffered most part of damage until overall collapse was reached as a result of masonry crushing at the pier bases. Different types of damage were observed on spandrels depending on their configuration (i.e., spandrel with wooden lintel or spandrel with masonry arch and RC bond beam) and their condition at the beginning of the test (i.e., as-built, pre-damaged, or IMG-repaired spandrel). Even a wooden lintel with low anchorage length in the spandrel of the as-built specimen #1 allowed the load transfer between the piers, because it forced the masonry to absorb and to dissipate input energy. This indicates that spandrels should be included in capacity models of URM buildings even if they do not include well-anchored lintels and RC bond beams according to current

seismic codes (ASCE 2000, CEN 2005, IBC 2008). A transition from shear to flexural cracking was detected in the case of the IMG-repaired spandrel, which suffered splitting at collapse. The IMG strengthening system behaved as an energy dissipation device for the spandrel panel. This allowed to restore load-bearing capacity of the as-built specimen #1, delaying strength degradation at larger displacements. No debonding of the IMG composite was detected because of its high compatibility with the masonry substrate. Reversibility and ease of use of the IMG strengthening system makes it an attractive tool for seismic protection of cultural heritage masonry buildings and urgent remedial works on damaged masonry buildings during earthquake sequences. Finally, the lateral loading test of specimen #2 showed a significantly different damage in the case of spandrels with masonry arch below and RC bond beam above. First cracks in the arch appeared at a drift level approximately equal to that associated with shear cracking in the spandrel with wooden lintel (specimen #1). As the drift of specimen #2 increased, a progressive collapse of the arch was observed and was followed by: (1) concrete cover ejection and plastic hinging in the RC bond beam; (2) progressive collapse of masonry layers above the arch; and (3) complete masonry crushing and splitting at the pier bases.

ACKNOWLEDGEMENT

This research was carried out in the framework of the ReLUIS-DPC 2010–2013 project (Line AT1-1.1 - ‘Evaluation of the Vulnerability of Masonry Buildings, Historical Centres and Cultural Heritage’) funded by the Italian Department of Civil Protection.

REFERENCES

- ASCE (2000). FEMA 356: Prestandard and commentary for the seismic rehabilitation of buildings, American Society of Civil Engineers, Washington, DC.
- Augenti, N. (2000). Il calcolo sismico degli edifici in muratura, UTET, Turin, Italy (in Italian).
- Augenti, N. and Parisi, F. (2009). Experimental data analysis on mechanical parameters of tuff masonry. *Second Workshop on Design for Rehabilitation of Masonry Structures*.
- Augenti, N. and Parisi, F. (2010). Constitutive models for tuff masonry under uniaxial compression. *Journal of Materials in Civil Engineering* **22:11**, 1102-1111.
- Augenti, N., Parisi, F., Prota, A. and Manfredi, G. (2011). In-plane lateral response of a full-scale masonry sub-assembly with and without an inorganic matrix-grid strengthening system. *Journal of Composites for Construction* **15:4**, 578-590.
- Augenti, N., Parisi, F. and Acconcia, E. (2012). MADA: online experimental database for mechanical modelling of existing masonry assemblages. *Fifteenth World Conference on Earthquake Engineering*, CD-ROM.
- Benedetti, D., Carydis, P. and Limongelli, M.P. (2001). Evaluation of the seismic response of masonry buildings based on energy functions. *Earthquake Engineering and Structural Dynamics* **30:7**, 1061-1081.
- CEN (1993). Eurocode 2: Design of concrete structures, Comité Européen de Normalisation, Brussels, Belgium.
- CEN (2005). Eurocode 8: Design of structures for earthquake resistance – Part 3: Assessment and retrofitting of buildings, Comité Européen de Normalisation, Brussels, Belgium.
- Gattesco, N., Macorini, L., Clemente, I. and Noè S. (2010). Shear resistance of spandrels in brick-masonry buildings. *Eighth International Masonry Conference*, CD-ROM.
- IMIT (2008). D.M. 14.01.2008: Norme Tecniche per le Costruzioni. Italian Ministry of Infrastructures and Transportation, Rome, Italy (in Italian).
- Magenes, G. and Calvi, G.M. (1997). In-plane seismic response of brick masonry walls. *Earthquake Engineering and Structural Dynamics* **26:11**, 1091-1112.
- Magenes, G., Penna, A. and Graziotti, F. (in print). Quasi-static cyclic testing of full-scale stone masonry spandrels, Report, IUSS Press, Pavia, Italy.
- Parisi, F. (2010). Non-linear seismic analysis of masonry buildings, PhD Thesis, University of Naples Federico II, Naples, Italy [URL: <http://wpage.unina.it/fulvio.parisi/>].
- Parisi, F. and Augenti, N. (2012). Seismic capacity of irregular unreinforced masonry walls with openings. *Earthquake Engineering and Structural Dynamics*, DOI: 10.1002/eqe.2195.
- Parisi, F., Lignola, G.P., Augenti, N., Prota, A. and Manfredi, G. (2011). Nonlinear behavior of a masonry subassembly before and after strengthening with inorganic matrix-grid composites. *Journal of Composites for Construction* **15:5**, 821-832.
- Prota, A., Marcari, G., Fabbrocino, G., Manfredi, G. and Caldea, C. (2006). Experimental in-plane behavior of tuff masonry strengthened with cementitious matrix-grid composites. *Journal of Composites for Construction* **10:3**, 223-233.